

# Impact response of textile-reinforced 3D printed concrete panels

Akilesh Ramesh <sup>a</sup>, Pathmanathan Rajeev <sup>a,\*</sup>, Shanqing Xu <sup>b</sup>, Jay Sanjayan <sup>a</sup>, Guoxing Lu <sup>b</sup>

<sup>a</sup> Centre for Sustainable Infrastructure and Digital Construction, Swinburne University of Technology, Australia

<sup>b</sup> School of Engineering, Department of Mechanical and Production Design Engineering Swinburne University of Technology, Australia

## ARTICLE INFO

### Keywords:

Impact  
High-strength concrete  
Failure pattern  
Energy absorption  
Drop load test

## ABSTRACT

This study assessed the impact response of 3D-printed textile-reinforced concrete for structural applications of 3D concrete printed structures, where impact is a significant load case. To study the impact response, two layers of AR-glass and two layers of carbon textile-reinforced 3D-printed high-strength concrete panels were investigated experimentally under low-velocity impacts from drop weights, respectively. The effect of textile reinforcement on the impact behaviour was compared with unreinforced printed specimens. The specimens were subjected to increasing levels of impact load until the failure was observed. The effect of textile reinforcement on the impact resistance, cumulative energy absorption capacity and failure pattern of printed specimens were investigated and compared with their mould-cast counterparts. To understand the effect of textile reinforcement on the printed and mould-cast panel specimens, a quasi-static flexural test was performed to evaluate the load vs deformation behaviour. The test results from the quasi-static flexural test showed that the incorporation of textile reinforcement improved the first crack strength by about 40 % and enhanced post-peak behaviour for both printed and mould-cast specimens. Further, providing carbon textile reinforcement significantly improved the impact resistance by 75 % when compared to AR glass textile-reinforced specimens due to the higher stiffness and better strain-hardening behaviour. Moreover, the effect of textile reinforcement on enhancing the energy absorption capacity of 3D-printed specimens was more evident at higher impact velocities. The cumulative energy absorption capacity of carbon textile-reinforced specimens was observed to be 60 % higher compared to AR glass textile-reinforced specimens. During high-velocity impacts, the textile reinforcement was observed to improve damage distribution by enhancing the bridging between the interlayers. The damage condition at failure showed that AR-glass textile-reinforced printed and mould-cast specimens showed severe punching failure on the compression face and widened cracks and spalling on the tension face. However, carbon textile reinforcement enhanced the impact resistance, thus showing multiple cracks and reduced spalling on the tension face even after multiple impacts. Overall, the impact performance of 3D-printed textile-reinforced concrete panels showed high-level impact resistance.

## 1. Introduction

3D concrete printing (3DCP) enables the construction of slender freeform structures with complex geometrical shapes and thus provides more freedom in designing aesthetically pleasing structural members [1–3]. However, developing high-strength printable concrete and providing effective reinforcement methods are some of the challenges that hinder the widespread structural application of 3DCP [4–6]. Unlike conventional concrete, the rheological properties of printable concrete for extrusion-based 3D printing need to be tailored in such a way that the mix has an initial low viscosity for good pumpability and high static yield strength development for better buildability [7–9].

To evaluate the structural potential of 3DCP members, it is important to characterise the mechanical properties. Moreover, 3D-printed concrete members showed anisotropic mechanical properties based on the printing direction [10–12]. However, to enhance the mechanical properties of printed members, various reinforcing methods were adopted in previous studies, including the use of short fibres (AR-glass, basalt, carbon and steel), carbon yarns, steel mesh reinforcement and pre-installed steel bars [13–16]. It is reported that short fibres of AR-glass and steel in concretes led to enhanced compressive strength and flexural capacity of 3DCP members and improved the hardening behaviour with directional dependency under quasi-static loading conditions [17–19]. However, the fibres tend to align uniformly along the

\* Corresponding author.

E-mail address: [prajeev@swin.edu.au](mailto:prajeev@swin.edu.au) (P. Rajeev).

<https://doi.org/10.1016/j.engstruct.2024.118489>

Received 11 December 2023; Received in revised form 15 June 2024; Accepted 20 June 2024

Available online 27 June 2024

0141-0296/© 2024 The Author(s). Published by Elsevier Ltd. This is an open access article under the CC BY license (<http://creativecommons.org/licenses/by/4.0/>).

printing direction in extrusion-based 3DCP, thus enhancing the post-peak behaviour when loading along the printing direction [13,20,21]. The structural performance of 3D-printed members was observed to be improved by providing steel mesh reinforcement and pre-installed steel bars, however, the rigidity of the steel reinforcement poses limitations on creating complex geometries with the 3DCP process [22]. Furthermore, concrete structures are subjected to both quasi-static and dynamic loading conditions. Therefore, it is essential to investigate the behaviour of 3DCP members under dynamic loading conditions in order to assess their overall structural potential.

The construction of slender and thin-walled structures is gaining popularity due to reduced material usage and the ability to build architecturally pleasing geometries. However, these structures are not only subjected to various static loads but also are subjected to various impact loads like debris from high wind, snow and blast loading [23]. The dynamic behaviour of conventional concrete under impact loading was studied extensively and the use of continuous textiles and discontinuous short fibres as reinforcement enhanced the impact resistance and energy absorption capacity [24]. The addition of short steel fibres as reinforcement in concrete slabs has shown to improve impact resistance with reduced crack widths [25,26]. Furthermore, the combination of polyethylene fibres and steel fibres as hybrid reinforcement enhances the blast resistance of concrete panels when compared with conventionally reinforced concrete panels [27]. However, the impact performance of discontinuous short fibre-reinforced concrete is not significantly enhanced and depends on the fibre orientation. In contrast, the adoption of continuous textile reinforcement provides reinforcement in both directions, making it ideal for improving the impact resistance of slender concrete structural members. Moreover, textile reinforcement may contribute to reducing the carbon footprint, making it suitable for the construction of novel structures with superior structural performance such as footbridges, complex roof elements, and façade slabs [28–30].

Textile-reinforced concrete exhibits enhanced first crack strength and improved toughness under quasi-static loading conditions [31]. Previous investigations on the dynamic tensile and flexural behaviour of textile-reinforced concrete members also showed improved mechanical properties and a reduction in cracking failure [32]. The impact behaviour under low-velocity drop-weight tests for textile-reinforced slab specimens depends on the number of textile layers, the type of textile reinforcement and the properties of the fine-grained concrete [33,34]. The flexural stress and energy absorption capacity were increased for textile-reinforced concrete panels with a predominant interlaminar shear failure [33]. However, with the addition of multiple textile layers, the impact resistance was found to be reduced due to delamination between the layers [34,35]. The studies on the impact behaviour of AR-glass textile reinforced concrete subjected to low velocity impacts demonstrated an increase in the peak impact load with increasing impact velocity, but no significant influence on the flexural capacity was observed [36]. Textile-reinforced concrete exposed to elevated temperature showed a reduction in the impact resistance and energy absorption capacity. However, the failure pattern under low velocity impact after exposed to elevated temperature showed a significant effect on AR-glass textile through a rupture failure of the fibres compared to basalt textile [37,38]. Furthermore, the impact behaviour of textile-reinforced concrete specimens under low velocity impact was significantly influenced by pre-tension, hybrid textiles and short fibres. Pre-tension improved the bonding to the cement matrix and enhanced the crack stress. The addition of short fibres improved the bridging of the micro cracks and thus enhanced the toughness of the textile reinforced specimens [39]. Moreover, hybrid textile-reinforced specimens showed enhanced impact resistance without significant improvement in the energy absorption capacity [40]. Thus, providing textile reinforcement not only improves the structural performance of concrete specimens under static loading but also enhances the impact behaviour.

Textile reinforcement enhances the structural performance of

concrete specimens and the flexibility and non-corrosive nature of textiles makes it as a potential reinforcing method for 3DCP structures. The flexural strength under quasi-static loading of AR-glass textile-reinforced 3D-printed specimens was found to be increased significantly and showed improved post-ductile behaviour [41–44]. However, the mechanical behaviour of 3DCP members under dynamic loading was briefly investigated only under compression. Unlike conventional concrete, 3DCP members showed significant variation in the direction-sensitive dynamic compressive strength. For example, the dynamic compressive strength of printed specimens was the highest when tested along the printing direction [45]. The effect of printing direction was more significant as compared with the sand to binder ratio of printed specimens when the dynamic compressive strength and energy absorption capacity was concerned. However, with the increase in the sand to binder ratio, the dynamic compressive strength and energy absorption capacity reduced [46]. Furthermore, similar to the anisotropic behaviour of 3D printed specimens under static loading, ultra-high performance fibre-reinforced 3DCP specimens subjected to dynamic loading exhibited anisotropy in the impact resistance, elastic modulus and failure pattern [47]. Based on previous studies, textile reinforcement improves the static and dynamic behaviour of concrete members. In addition, textile-reinforced 3D-printed members showed enhanced load carrying capacity and flexural toughness under static loading. However, the dynamic behaviour of textile-reinforced 3D-printed structures needs further investigation.

Therefore, the impact response of textile-reinforced 3D-printed high-strength concrete slender panels subjected to dynamic loads was investigated in this study. To evaluate the effect of textile reinforcement on the impact resistance, energy absorption capacity and failure patterns, multiple impact tests were conducted on the same specimen from two different drop heights (1 m and 2 m). Additionally, the effect of two layers of AR-glass textile and two layers of carbon textile reinforcement on the flexural impact behaviour of concrete slabs were investigated and were compared to their mould-cast counterparts. The failure mode and crack pattern after failure due to multiple drops were analysed using high-speed camera recordings. Furthermore, the effect of textile reinforcement on the quasi-static flexure behaviour was also evaluated to characterise the impact behaviour of printed and mould-cast specimens.

## 2. Materials and mix proportion

### 2.1. Materials

The binder materials for the high-performance concrete consist of OPC, silica fume and slag conforming to AS 3972 [48] and AS 3582 [49], respectively. The 3D printable concrete and mould-cast concrete mix also consists of three different sieve-graded silica sands as aggregates and are categorised as fine, medium, and coarse sand with their mean particle sizes of 273.2  $\mu\text{m}$ , 469.5  $\mu\text{m}$ , and 1735.8  $\mu\text{m}$ , respectively. The particle size distribution was performed by sieve analysis according to ASTM C136 [50] for sand and laser ultrasonic technique for binders, as illustrated in Fig. 1. In addition, polycarboxylate ether (PCE) based superplasticizer (SP) and viscosity modifying agent (nano clay) conforming to AS 1478.1 [51] were used to control the workability and rheological properties of the concrete mix.

Commercially available AR-glass textile and carbon textile as shown in Fig. 2 were used as reinforcement for both 3D printed and mould-cast panel specimens. The textile reinforcement is composed of multi-filament fibre yarns aligned along both longitudinal and transverse directions. The longitudinally aligned fibre yarns corresponds to the 'warp' yarns, while the fibre yarns aligned along the transverse direction represents the 'weft' yarns as marked in Fig. 2. The physical properties of both the textile reinforcements are given in Table 1. The tensile strength of the warp yarns given in Table 1 represents the strength of five yarns tested under tension and the strength is represented in N/50 mm.

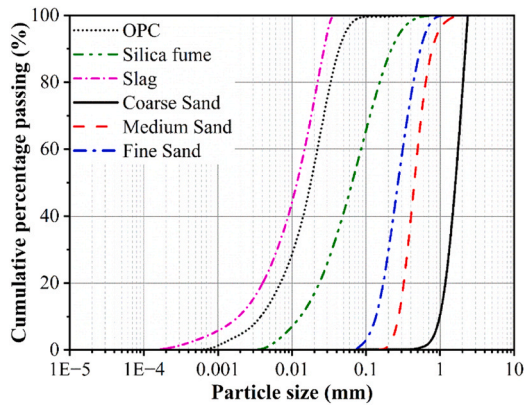


Fig. 1. : Particle size distribution for sand and binder materials.

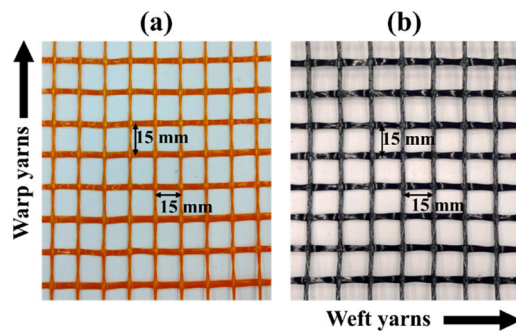


Fig. 2. : (a) AR-glass textile and (b) Carbon textile.

## 2.2. Mix proportion

The details of the mix proportion for the 3D printable and mould-cast high-performance concrete adopted in this study are given in Table 2. Initially, all the dry materials were slowly mixed for two minutes in a 60 L capacity planetary mixer. Then, SP was mixed with 70 % of the water and added slowly to the mixer while continued mixing at a slow speed (i.e., 70 rpm) for another five minutes. After adding the remaining amount of water, the mixing was continued for about three minutes at the same speed of 70 rpm. Lastly, nano-clay was added to the mixture and continued mixing for another five minutes at high speed (i.e., 190 rpm). The concrete mixture was observed to have good printable properties.

Table 1  
Properties of the textile reinforcements\*.

Textile	Mesh size (mm × mm)	Weight (g/m <sup>2</sup> )	Area of warp yarns per 100 mm width (mm <sup>2</sup> )	Tensile strength of five warp yarns (N/50 mm)	Modulus of elasticity (GPa)	Thickness of yarn (mm)
AR glass	15 × 15	335	12.37	3100	72	1.5
Carbon		408		4950	215	

\* Provided by the supplier

Table 2  
Mixture proportion.

OPC	Slag	Silica fume	Fine sand	Medium sand	Coarse sand	Water <sup>#</sup>	SP <sup>#</sup>	Nano clay <sup>#</sup>
0.595	0.105	0.3	0.4	0.3	0.3	0.2	0.01	0.002

<sup>#</sup> All values are mass ratios to the binder

## 3. Specimen preparation

The impact resistance of 3D-printed and mould-cast high-performance concrete was evaluated by preparing square panels of 330 × 330 × 30 mm. As shown in Fig. 3, a gantry-type 3D printer with a printing region of 1800 × 1600 × 1800 mm was used to prepare 3D-printed concrete panels.

The concrete panels were printed using a 30 mm diameter circular nozzle attached to the extruder. The extruder was programmed to move along the X-axis and Y-axis at a constant speed of 30 mm/s. After completion of one layer, the extruder moved by 5 mm along the Z-axis to print the next layer. The printed panel specimens consists of total 6 layers of high-performance concrete printed as explained in the above mentioned pattern to form an overall specimen thickness of 30 mm. Additionally, to maintain a constant width of the printed filament, the auger extrusion rate was modified between 0.5 to 0.7 rad/s throughout the printing process. In the reinforced printed specimens, two layers of textile reinforcement were laid manually in between the first and second layers (the first textile layer) and the fifth and sixth layers (the second textile layer), as shown in Fig. 4(a). The printing process was temporarily paused to place the textile reinforcement, and in order to ensure a uniform bond, the placed textile was subsequently rolled over the printed layer. In mould-casting process, plywood moulds were used to prepare the panel specimens. Textile reinforcements were positioned at 5 mm from both the bottom and top and was securely held in position. Subsequently, the concrete mix was poured in three distinct layers and compacted within each layer for 2 min using a vibration table. Proper care was taken to prevent the formation of air voids and inadvertent displacement of the textile reinforcement. The details of the mould-cast specimens are shown in Fig. 4(b).

A total of 36 panels were printed and mould-cast, including two repeats of the same testing conditions. The details of the specimens and testing conditions are summarised in Table 3. Both the printed and mould-cast specimens were covered and left for 48 h at room temperature of 23±3 °C before demoulding (mould-casting) or removal from the platform (3D printing). Afterwards, both printed and cast specimens were submerged in water and placed in the oven at 90 °C for 48 h to expedite steam curing. Following the curing process, the specimens were left at room temperature for about 72 h. As such, a total curing duration of 7 days was adopted in this study to achieve accelerated strength development for the panel specimens.

## 4. Experimental methods

### 4.1. Properties of high-performance concrete mix

To evaluate the workability, rheological and mechanical properties of the high-performance concrete mix used in this study, the spread diameter, the plastic viscosity, the yield strength and compressive

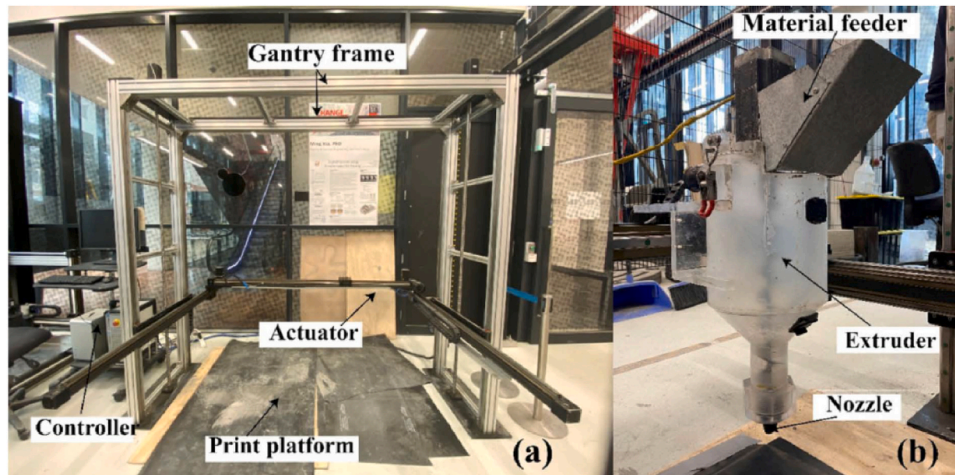


Fig. 3. (a) Gantry type 3D printer (b) Extruder and nozzle.

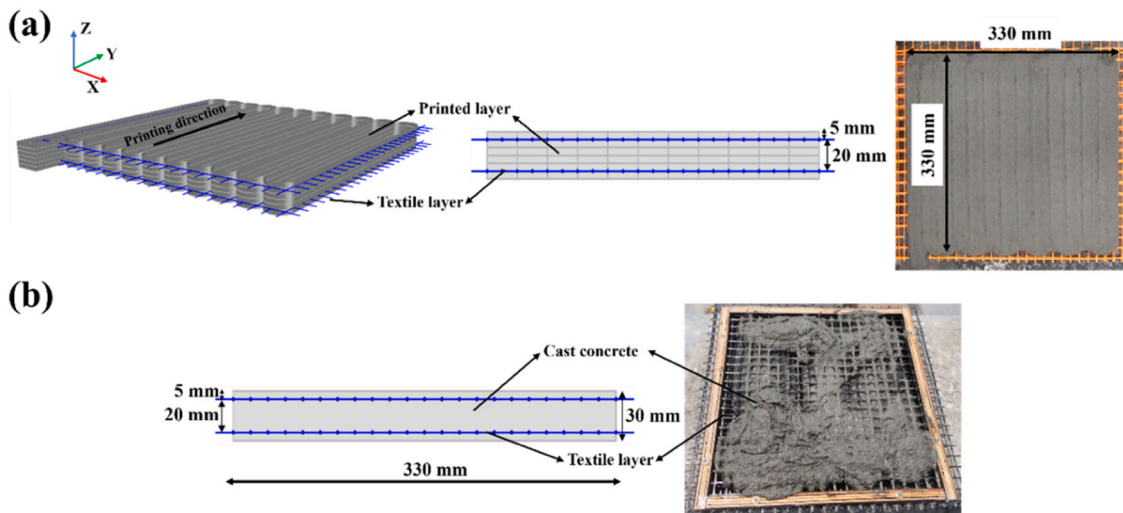


Fig. 4. : Textile reinforced concrete panel specimens fabricated by (a) 3D printing (b) mould-casting.

Table 3  
Summary of specimens and test conditions.

Specimen id	Type of textile	Preparation process	Drop height (m)
P-0 T-H1	No textile	3D-printed	1
C-0 T-H1		Mould-cast	
P-GT-H1	AR-glass	3D-printed	
C-GT-H1		Mould-cast	
P-CT-H1	Carbon	3D-printed	
C-CT-H1		Mould-cast	
P-0 T-H2	No textile	3D-printed	2
C-0 T-H2		Mould-cast	
P-GT-H2	AR-glass	3D-printed	
C-GT-H2		Mould-cast	
P-CT-H2	Carbon	3D-printed	
C-CT-H2		Mould-cast	
P-0 T-Static	No textile	3D-printed	Static test
C-0 T-Static		Mould-cast	
P-GT-Static	AR-glass	3D-printed	
C-GT-Static		Mould-cast	
P-CT-Static	Carbon	3D-printed	
C-CT-Static		Mould-cast	

Note: Specimen id P-GT-H2 represents a printed panel with AR-glass textile reinforced and a drop height of 2 m. P and C represent printed and mould-cast panels, 0 T, GT and CT represent no textile, AR-glass textile and carbon textile, and the last term indicates the drop height.

strength values were measured. A flow table test according to ASTM C1437 [52] was carried out to evaluate the workability of the concrete mix. The spread diameter across two perpendicular directions of the concrete mix was measured both before and after subjecting to 25 drops on the flow table. To assess the rheological properties, a rotational rheometer was employed and a shearing protocol similar to that in the previous studies of the authors was used to determine the flow curve [14]. The obtained torque and rotational velocity data from the rheometer were converted into shear stress and shear rate using the Reiner-Rwlin equation [53]. Three measurements were taken to ensure the homogeneity of the data and the average values were reported.

To characterise the compressive strength of the high-performance concrete mix, cube specimens of 50 mm in dimension were tested under a quasi-static loading rate of 0.33 MPa/s using a uniaxial compression testing machine. The compression test was performed on the cube specimens that are saw-cut from printed panels for 3D printed specimens and from 50 mm cube moulds for mould-cast specimens. It should be noted that to evaluate the anisotropic behaviour of 3D printed specimens, compression tests were performed in three different directions [13,14].

#### 4.2. Quasi-static flexural test of panels

To evaluate the static behaviour of 3D-printed and mould-cast

textile-reinforced concrete panels,  $330 \times 330 \times 30$  mm panels were tested using a spherical indenter of the diameter 62.5 mm with a quasi-static loading velocity of 1.0 mm/min, as shown in Fig. 5. The specimens were pin supported on all the four sides of a rigid base frame. The test continued until no further increase in load readings was observed or the specimen failed from spalling or widened cracks. The load and corresponding mid-span deflection were measured and recorded.

### 4.3. Drop load impact test

Fig. 6 displayed the setup of the drop weight impact test. The drop tower consists of a steel support frame for the specimen, a spherical indenter of the same diameter, 62.5 mm, as quasi-static flexural tests, a loading mass which may drop freely along the guide rails on the two sides of the tower, a carriage which carries the dropping mass, and a Kistler load cell with the load capacity of 100 kN. The dropping mass was locked on the carriage, which can be raised to the desired height using a hoisting rope. In this study, the dropping mass was 8 kg including the indenter and the loading frame. After locking the dropping mass, the carriage was lifted to the desired drop height. Once the carriage is raised to the desired height, the locking device is triggered to release the mass, which drops freely along the two guide rails to impact with the specimen installed on the support frame.

The specimen is pinned supported on all the four sides of a rigid steel support frame of the size  $400 \times 400 \times 75$  mm<sup>2</sup> with an impact window of  $300 \times 300$  mm<sup>2</sup>. The steel support frame was bolted on the Kistler load cell fixed on the base to measure the impact force. The force signal from the load cell is recorded using a Tektronix MDO34 oscilloscope with 200 MHz bandwidth. In order to measure the mid-span deflection of the specimen during the impact, an accelerometer with a sensitivity of 0.264 mV/g was fixed on the bottom surface of the specimen. The accelerometer readings were double integrated to obtain the deflection at the mid-span to the corresponding impact force. To capture the failure mode of the specimens from the impact, a high-speed camera was placed right in front of the drop tower and recorded the deformation and cracking procedure at a frame rate of 10,000 frames per second. In the experiments, each type of specimens was dropped from two different heights of 1 m and 2 m, resulting in an impact velocity of 4.43 m/s and 6.26 m/s, respectively. The impact force, deflection at peak force, energy absorption and failure mode were analysed based on the collected data. For every impact velocity, multiple drops were performed until specimen failure.

## 5. Results and discussion

### 5.1. Properties of the mix

Table 4 summarises the workability, rheological properties and compressive strength of the high-performance concrete used in this study. The flow diameter before drop was observed to be close to the bottom diameter of the flow cone, showing good shape retention behaviour of the mix during the printing process. Furthermore, after

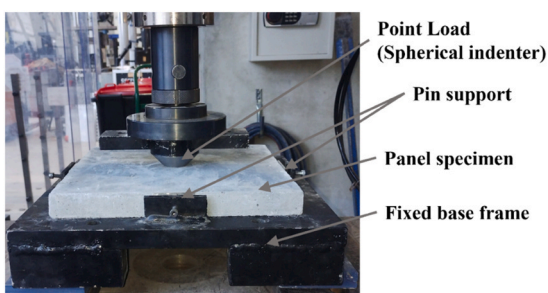


Fig. 5. : Quasi-static flexural test setup.

subjecting the mix to 25 drops on the flow table, there was a noticeable increase in the flow diameter, indicative of reasonably good workability. Nevertheless, the increase was not significant, highlighting the resistance of the concrete to withstand the load imposed by the subsequent printed layers. These findings are consistent with similar observations on the flow diameter results for printable mix in previous studies [9]. In addition, the viscosity and yield strength values of the high-performance mix adopted in this study imply its suitability for good pumping [54].

The compressive strength of the 3D-printed high-performance concrete specimens exhibited anisotropic behaviour in relation to the printing direction. Notably, the compressive strengths along the X and Y directions closely resembled to that of the mould-cast specimens, which quantifies to the effective compaction of the printed layers from the extrusion pressure. Similar anisotropic mechanical characteristics in printed specimens have been previously reported in prior researches [13,55].

### 5.2. Quasi-static flexural behaviour

Fig. 7 illustrates the load vs deflection behaviour of both 3D-printed and mould-cast concrete panels subjected to quasi-static flexural loading. Under the quasi-static flexural loading condition, both printed and mould-cast specimens displayed similar load vs deflection curve and failure patterns. However, when comparing the C-0 T-Static and P-0 T-Static specimens with their counterparts reinforced with AR-glass and carbon textiles, a significant improvement was observed in the first crack load and post-cracking behaviour. As shown in Fig. 7(a), specimens without textile reinforcement demonstrated a deflection softening behaviour, whereas their textile-reinforced counterparts, both printed and mould-cast displayed a deflection hardening behaviour. Nevertheless, the P-0 T-Static specimens exhibited a 38 % increase in deflection at the first crack load compared to the C-0 T-Static specimens. This difference can be attributed to the presence of interlayers in the printed specimens, which delays the attainment of their tensile strain capacity during the elastic range.

However, after the formation of the first crack, printed specimens showed lower post-peak load-carrying capacity, along with larger deformations and spalling at the point of failure. In contrast, the mould-cast specimens displayed uniform crack propagation and a slightly higher post-peak load-carrying capacity compared to their printed counterparts. In addition, it can be seen that the first crack load for both 3D-printed and mould-cast specimens was about 5.9 kN. However, with the incorporation of textile reinforcement the first crack load was increased by 61 % for AR-glass textile and 72 % for carbon textile for both 3D-printed and mould-cast specimens, respectively.

The addition of textile reinforcement significantly enhanced the overall flexural stiffness of the concrete panels, resulting in improved load-carrying capacity. The improved flexural stiffness of textile-reinforced specimens was evident with carbon textile reinforcement due to their higher tensile strength and elastic modulus and resulted in improved load carrying capacity at larger deflection. However, it is to be noted that some of the printed and mould-cast specimens reinforced with carbon textile showed a sudden reduction in strength after reaching peak load. This can be attributed to fracture of some of the carbon textile filament yarns and debonding of carbon yarns due to the increased tensile strain at the textile and higher bond stress at the interface [56]. Notably, the first crack load for the P-GT-Static specimen exceeded that of the C-GT-Static specimen by 17 %, while the deflection at first crack load remained similar. However, carbon textile-reinforced printed and mould-cast specimens were observed to have comparable first crack load and first crack deflection. The increase in the first crack behaviour can be attributed to the enhanced composite behaviour from the improved bond between textile and concrete [56]. Furthermore, the enhanced post-peak behaviour of textile-reinforced printed specimens is due to the improved interlayer bridging with the textile delaying the failure.

Furthermore, the peak load-carrying capacity and total energy

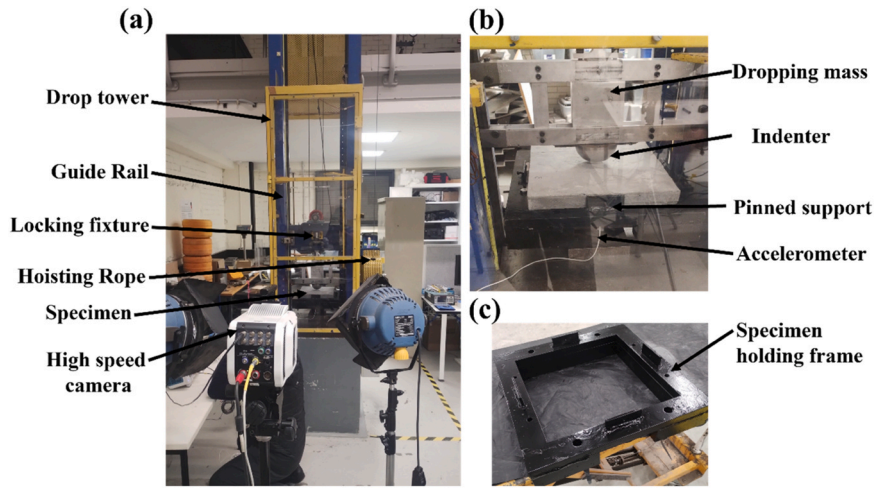


Fig. 6. : Drop weight test set-up (a) full setup (b) enlarged view of impact region (c) holding frame.

Table 4  
Properties of the high-performance concrete mix (error indicates mean ± one standard deviation).

Spread diameter (mm)		Rheology		Compressive strength (MPa)			
Before drop	After drop	Viscosity (Pa.s)	Yield strength (Pa)	Cast	Printed direction		
				X	Y	Z	
105	132	55.7 ± 2.6	355.8 ± 16.9	116.9 ± 5.0	114.7 ± 4.2	112.3 ± 3.8	97.5 ± 2.4

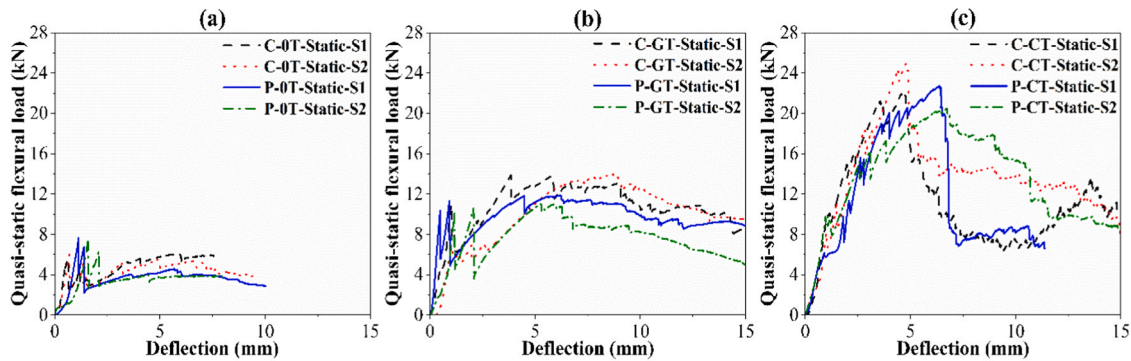


Fig. 7. : Quasi-static flexural load vs deflection of printed and mould-cast specimens (a) No textile (b) AR-glass textile (c) Carbon textile.

absorbed during the quasi-static flexural loading condition for both the printed and mould-cast concrete panels are depicted in Fig. 8. Regardless of the textile reinforcement, the peak load and the total energy absorption capacity of both printed and mould-cast specimens were observed to be similar. However, the presence of textile reinforcement significantly improved the load carrying capacity and the total energy absorption. The energy absorption capacity of concrete panels were measured from the area under the load-deflection curve until 10 mm deflection. It was observed that, unreinforced panels showed a maximum deflection of 10 mm under quasi-static flexural loading. Furthermore, the total energy absorption capacity of P-0 T-Static specimens was observed to be lower than C-0 T-Static specimens which can be attributed to the pronounced deflection softening behaviour observed in case of printed specimens. Nonetheless, the addition of textile reinforcement improved the post-peak deflection hardening behaviour of printed specimens resulting in comparable energy absorption capacity and peak load to that of mould-cast specimens.

Moreover, the C-CT-Static and P-CT-Static specimens demonstrated improved the peak load capacity of 78 % and energy absorption capacity of 50 % when compared to the C-GT-Static and P-GT-Static specimens.

The higher tensile strength and elastic modulus of carbon textile reinforcement compared to AR-glass textile reinforcement resulted in enhanced bending stiffness and improved post-peak behaviour. Thus, providing textile reinforcement enhances the post-peak behaviour for 3D-printed specimens under quasi-static loading conditions.

### 5.3. Impact response of panels

#### 5.3.1. First drop impact response

To understand the impact behaviour, a typical impact force vs time graph of a specimen is shown in Fig. 9. The typical impact response can be divided into two stages: the impact region (the impact between indenter and specimen) and the springing region (after the rebound of dropping mass).

After the point of contact between indenter and the specimen, the impact force increases linearly until reaching the peak load. The peak impact force corresponds to the rate of change of momentum of the dropped weight. However, it has to be noted that the peak impact force depends on the elastic stiffness, inertia of the slab and the surface roughness [57,58]. To mitigate the losses from the contact between the

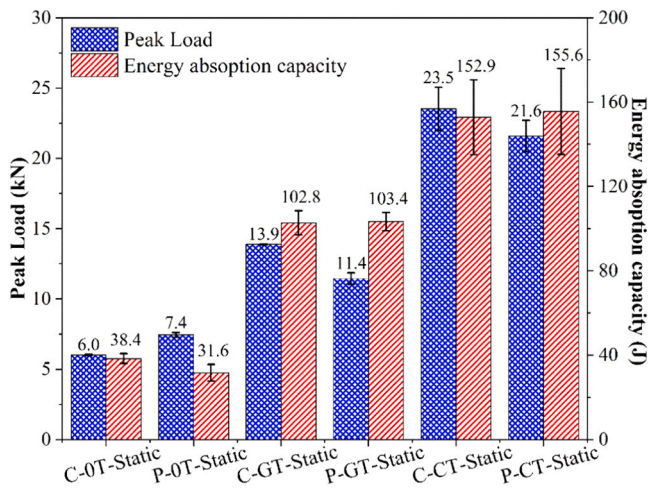


Fig. 8. : Maximum load and Energy absorption capacity of specimens under quasi-static loading (error bar indicates mean ± one standard deviation).

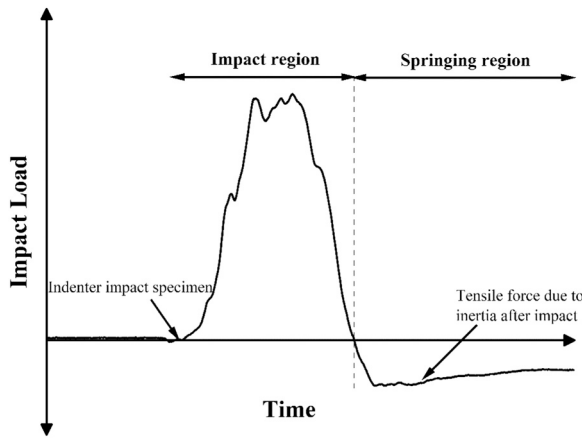


Fig. 9. : Typical impact force vs time behaviour.

indenter and the specimen, the top surface of the specimens are smoothed. After reaching the initial peak impact force, the indenter further deforms the specimen with the remaining momentum. However, during this phase, the specimen and head oscillate at different frequency which can be noted as fluctuations in the impact force vs time curve. Later on, after undergoing sufficient deformation, the indenter and the panel rebounds back to the initial position, causing the impact force to drop to zero. However, due to the effect of inertia in the impact, the specimen and the supporting frame mounted on the load cell tend to experience a tensile force which is marked by the negative force value due to the springing after impact.

Figs. 10 and 11 show the impact force vs deflection behaviour for all

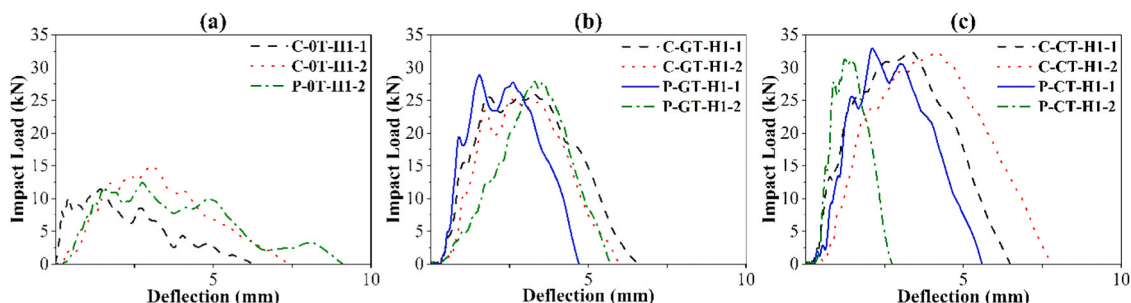


Fig. 10. : First drop impact behaviour of printed and mould-cast specimens for 1 m drop height (a) No textile (b) AR-glass textile (c) Carbon textile.

the specimens dropped from a height of 1 m (4.43 m/s velocity) and a height of 2 m (6.26 m/s), respectively. The impact behaviour for both the drop heights showed a similar mode for both printed and mould-cast specimens. It is to be noted that the oscillations from the accelerometer after the impact (during the springing region) were not considered in calculating the deflection as it may lead to misinterpretation.

The peak impact force for both printed and mould-cast specimens showed similar behaviour for both the drop velocities regardless of the textile reinforcement. However, the specimens with textile reinforcement showed higher impact resistance attributed to the increased stiffness of the panels. Similar observations were reported in previous studies with textile-reinforced slabs under low velocity impact [34,36, 38]. Moreover, the specimens reinforced with carbon textile showed higher impact resistance than AR-glass textile due to the higher tensile strength. The peak impact force increased by 94.9 % and 67.7 % for AR-glass textile reinforced specimens and by 132.5 % and 173.4 % for carbon textile reinforced specimens when compared to unreinforced concrete panels impacted by a mass dropped from both 1 m and 2 m, respectively. Furthermore, the printed specimens displayed slightly higher deformation than the mould-cast counterparts, indicating increased energy dissipation, especially at higher impact velocities. Furthermore, the presence of interlayers distributes the impact force for printed specimens, unlike homogeneous mould-cast specimens. In addition, the deformation after each impact was observed to be slightly higher for printed specimens and the failure load and deformation are improved for printed specimens due to the presence of interlayers. Moreover, the addition of textile reinforcement in the printed specimens improved the distribution of the impact force between the printed layers, leading to an overall improvement in the impact behaviour.

The damage caused by the first impact is shown in Fig. 12 for both drop heights. The addition of textile reinforcement improves the stiffness of the concrete panels and enhances the impact resistance. It can be observed from Figs. 12(a) and 12(b) that, specimens without textile reinforcement exhibited crack propagation from the point of impact and showed brittle failure after the initial impact. However, textile-reinforced specimens showed no discernible damage at a drop height of 1 m and exhibited minor crack formation near the support region in the case of a drop height of 2 m. Moreover, in contrast to AR-glass textile reinforced panel specimens, those reinforced with carbon textile displayed no visible damage following the first impact, even when subjected to a higher drop height. However, the formation of micro cracks during the impact is possible even with textile reinforcement. The enhanced stiffness and higher tensile strength of carbon textile when compared to AR-glass textile resulted in enhanced impact resistance even under higher drop velocity. In addition, it can be observed that spalling and cracks occur between the interlayers for the P-0 T-H1 and P-0 T-H2 specimens. Moreover, under higher drop height due to the increased impact force, the interlayer bond gets weakened resulting in delamination of layers as observed in Fig. 12(b). However, panel specimens reinforced with textile demonstrated reduction in the interlayer damage, attributed to the improved bridging effect between the printed layers and more effective distribution of the impact force.

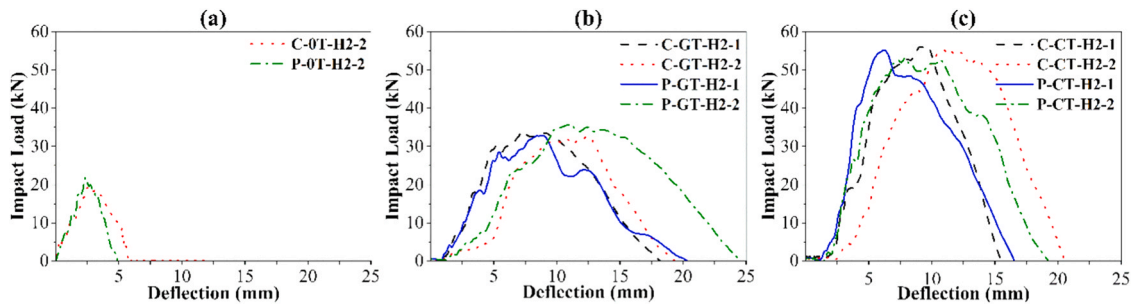


Fig. 11. : First drop impact behaviour of printed and mould-cast specimens for 2 m drop height (a) No textile (b) AR-glass textile (c) Carbon textile.

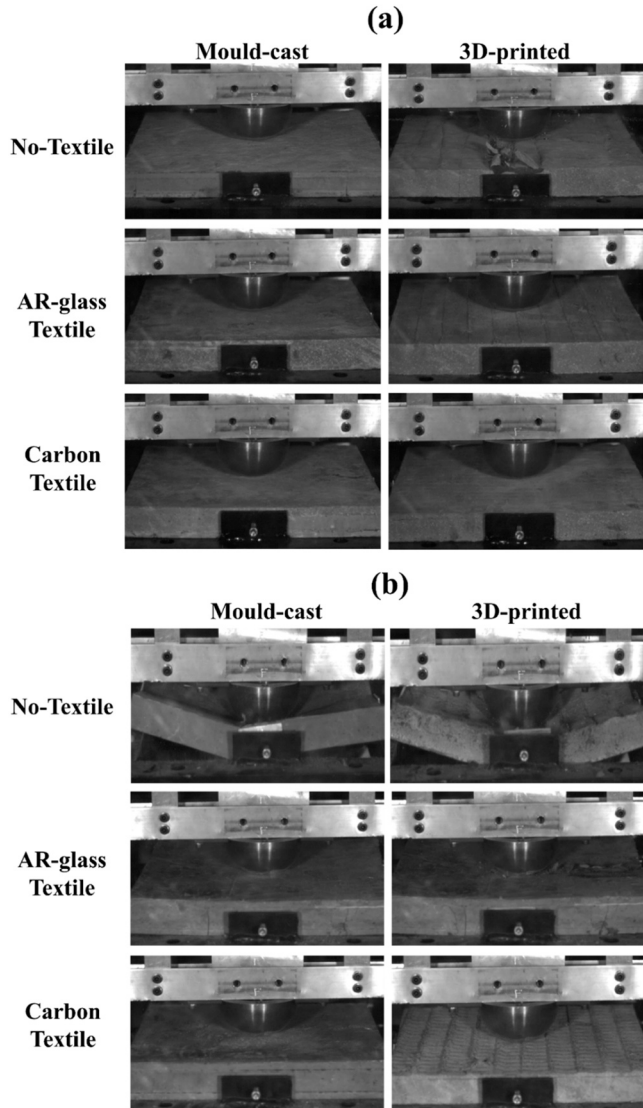


Fig. 12. : Failure mode after first impact for (a) 1 m drop height (b) 2 m drop height.

5.3.2. Multiple drops impact response

The impact resistance and the cumulative energy for textile-reinforced concrete panels for both drop heights are presented in Fig. 13 and Fig. 14. In contrast to unreinforced concrete panels, both printed and mould-cast specimens with textile reinforcement did not fail after the first drop. Consequently, the drop weight was released multiple times from corresponding heights until failure. The failure of the panels was determined by a sudden drop in the impact force or the occurrence

of widened cracks and concrete spalling. The cumulative energy after each drop was calculated as the area under the impact force vs deformation curve during the impact region.

In Fig. 13(a), it is evident that the impact resistance of carbon textile-reinforced concrete panels was higher than that of AR-glass textile-reinforced specimens. Furthermore, carbon textile-reinforced specimens maintained nearly consistent impact resistance force for up to 5 drops. This might be attributed to the higher stiffness of the carbon textile-reinforced specimens, demonstrating pronounced deflection hardening behaviour under flexure and thus under low impact velocities (4.43 m/s) improves the impact resistance. The energy required to induce higher tensile strains for crack development was achieved after a greater number of drops. However, specimens reinforced with AR-glass textile exhibited widened cracks and spalling, resulting in reduced impact resistance after 3 drops. In addition, that the experimental results revealed similar impact resistance capacities for both printed and mould-cast specimens. The higher tensile strength of textile reinforcement facilitated bridging between the interlayers, improving the composite behaviour of the textile reinforced panels in distributing the impact forces.

Fig. 13(b) revealed a comparable variation in the cumulative energy for both printed and mould-cast specimens. However, due to the higher number of drops required for carbon textile-reinforced specimens, the total cumulative absorbed energy was greater. The C-GT-H1 and the P-GT-H1 panel specimens exhibited lower impact resistance compared to their carbon textile-reinforced counterparts. Nevertheless, the cumulative energy absorbed up to 6 drops was similar, because of the larger deformation of AR-glass textile-reinforced specimens under impact loading, attributed to their lower stiffness. A similar trend was not observed when the impact velocity increased.

An increase in the impact velocity from 4.43 m/s to 6.26 m/s increases the kinetic energy by 2 times. The panel specimens subjected to higher impact velocities experience greater tensile forces at the bottom of the panels and get amassed with an increasing number of drops. Consequently, the impact resistance capacity of textile-reinforced specimens is reached from a lower number of impacts under higher impact velocity loading conditions. Observing Fig. 14(a), it was noted that both textile-reinforced specimens failed after 3 drops when impacted by a mass dropped from 2 m. In addition, the impact resistance capacity reduced linearly for both printed and mould-cast specimens. Fig. 14(b) also illustrated that the cumulative energy absorption of carbon textile-reinforced specimens was higher than that of AR-glass textile-reinforced specimens. The higher tensile strength of carbon textile increases the impact resistance by about 75 % as compared with AR-glass textile under higher impact velocities. The enhanced composite behaviour of panels specimens reinforced with carbon textile leads to enhanced impact performance and an increase in the energy absorption capacity. Moreover, printed specimens exhibited higher deformations compared with mould-cast specimens under higher impact velocities. It is evident that textile reinforcement significantly enhances the impact resistance for both printed and mould-cast specimens, especially under higher impact velocities.

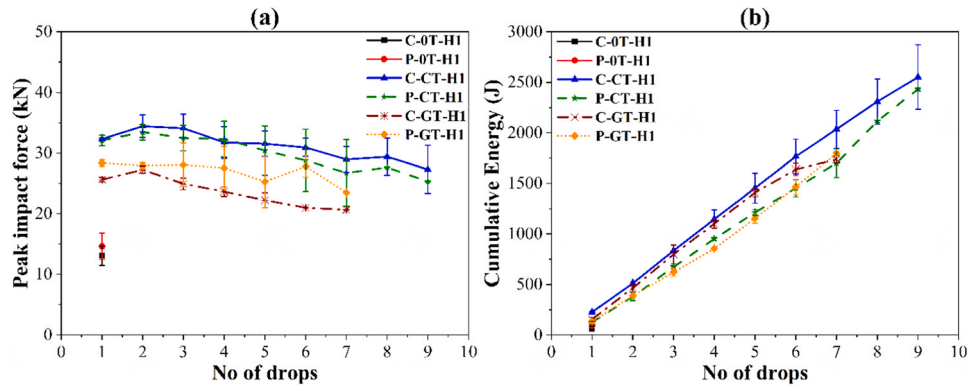


Fig. 13. : Impact response of different concrete panels after multiple drops from 1 m height (a) Peak impact force, (b) Cumulative energy after each drop (error bar indicates mean  $\pm$  one standard deviation).

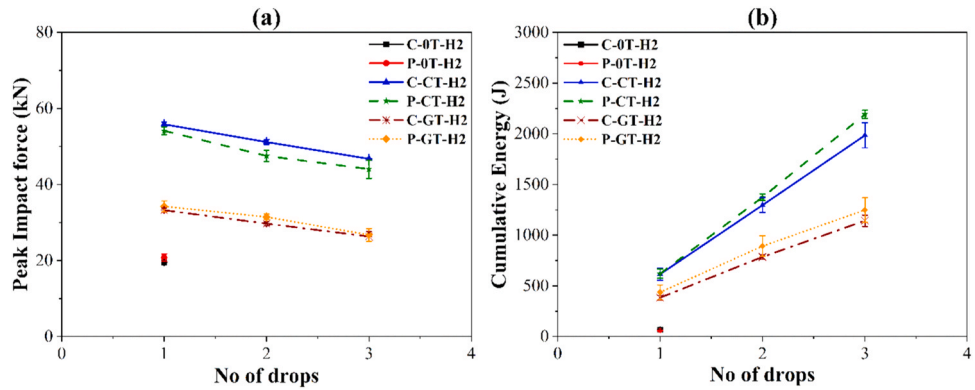


Fig. 14. : Impact response of different concrete panels after multiple drops from 2 m height (a) Peak impact force, (b) Energy absorption capacity (error bar indicates mean  $\pm$  one standard deviation).

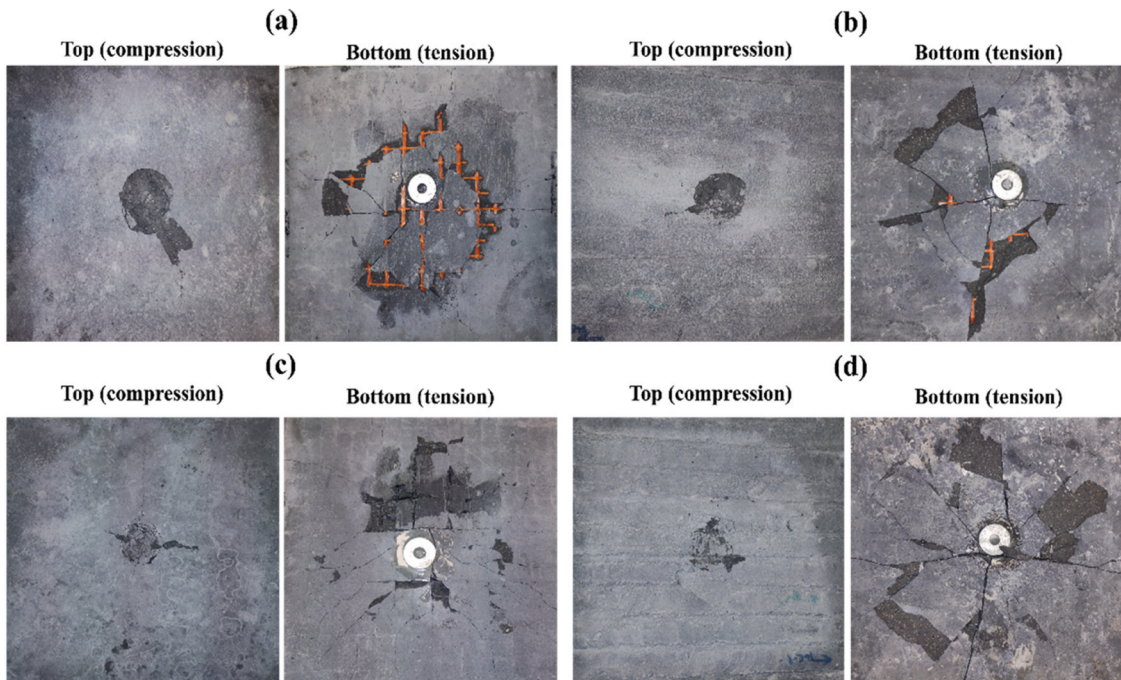


Fig. 15. : Top and bottom view of failure pattern after final impact (a) C-GT-H1 (b) P-GT-H1 (c) C-CT-H1 (d) P-CT-H1.

The failure pattern of textile-reinforced printed and mould-cast specimens after multiple drops from both impact velocities are shown in Fig. 15 and Fig. 16. In case of specimens reinforced with AR-glass textile, distinct flexural cracks on the tension phase at failure was evident, as depicted in Figs. 15(a) and 15(b). The flexural cracks, occurring after multiple impacts was observed to form in the centre of the slab propagating towards the four supports. Moreover, localised tensile failure with spalling of concrete was observed for both printed and mould-cast specimens following multiple impacts. In contrast, Figs. 15(c) and 15(d) reveal that carbon textile-reinforced printed and mould-cast specimens exhibited multiple cracks under failure on the tensile phase, radially propagating from the centre towards the supports. The pronounced deflection hardening behaviour of carbon textile reinforced panel specimens can be attributed to the formation of multiple cracks under failure with minimised concrete spalling. Furthermore, in contrast to carbon textile reinforced specimens, AR-glass textile reinforced specimens exhibited significant punching failure from the indenter on the compression side.

In Figs. 16(a) to 16(d), it is evident that higher impact velocities lead to severe damage, manifested through excessive spalling and widened cracks with a lower number of impacts. Both the printed and mould-cast specimens, reinforced with both textiles, exhibits a failure pattern characterised by significant crushing and widened cracks on the compressive side under higher impact velocities. Moreover, the crushing failure and tensile cracks for printed specimens were observed to be reduced when reinforced with carbon textile. This is attributed to the higher tensile strength and elastic modulus of carbon textile, which improves the distribution of impact force under higher velocity impacts. Consequently, this results in minimised crack width and spalling. Thus, providing high-strength textile reinforcement for printed specimens not only improves impact resistance but also resists crack propagation and failure during higher impacts.

## 6. Conclusions

The impact resistance capacity of textile-reinforced 3D concrete printed panels in comparison with their mould-cast counterparts was investigated in this study under the drop weight impact test. Further, the

effect of textile reinforcement on the impact behaviour was evaluated by comparing the behaviour of unreinforced printed and mould-cast panels. The impact load from multiple drops and the cumulative energy absorbed were evaluated for all the specimens subjected to two different impact velocities. Further, the effect of textile reinforcement on the failure mode and crack propagation of printed and mould-cast panels were also compared from the experimental results. From the experimental results observed from this study, the following conclusions were drawn:

- The impact load vs deformation behaviour for both the printed and mould-cast panel specimens were observed to be similar for both the drop heights. However, the deformation of the printed panels from the impact was observed to be slightly higher than that of the mould-cast panels due to the presence of interlayers, which increases their energy dissipation capacity. Further, providing carbon textile reinforcement improved the impact resistance for both printed and mould-cast specimens significantly and controlled crack propagation and failure.
- Further, the quasi-static flexural test shows providing textile reinforcement improved the first crack load by 36 % for AR-glass textile and 45 % for carbon textile and also showed enhanced post-hardening behaviour and improved failure load carrying capacity. The enhanced post-hardening behaviour of both textile-reinforced panels was observed to enhance the impact behaviour from the damage condition from the first impact. Unlike unreinforced specimens, for a drop height of 1 m, there was no damage observed for the textile-reinforced specimens whereas minor cracks were observed for the drop height of 2 m.
- The impact resistance after multiple drops for the C-CT-H1 and P-CT-H1 specimens was observed to show a significant reduction and widening of cracks after 5 drops. However, the C-GT-H1 and P-GT-H1 specimens showed a reduction of impact resistance and failure occurred after 3 drops. The higher stiffness and enhanced deflection hardening behaviour from carbon textile reinforcement improved the impact resistance of the panels significantly. However, the cumulative energy absorption capacity of both the textile-reinforced panels for the drop height of 1 m was observed to vary similarly.

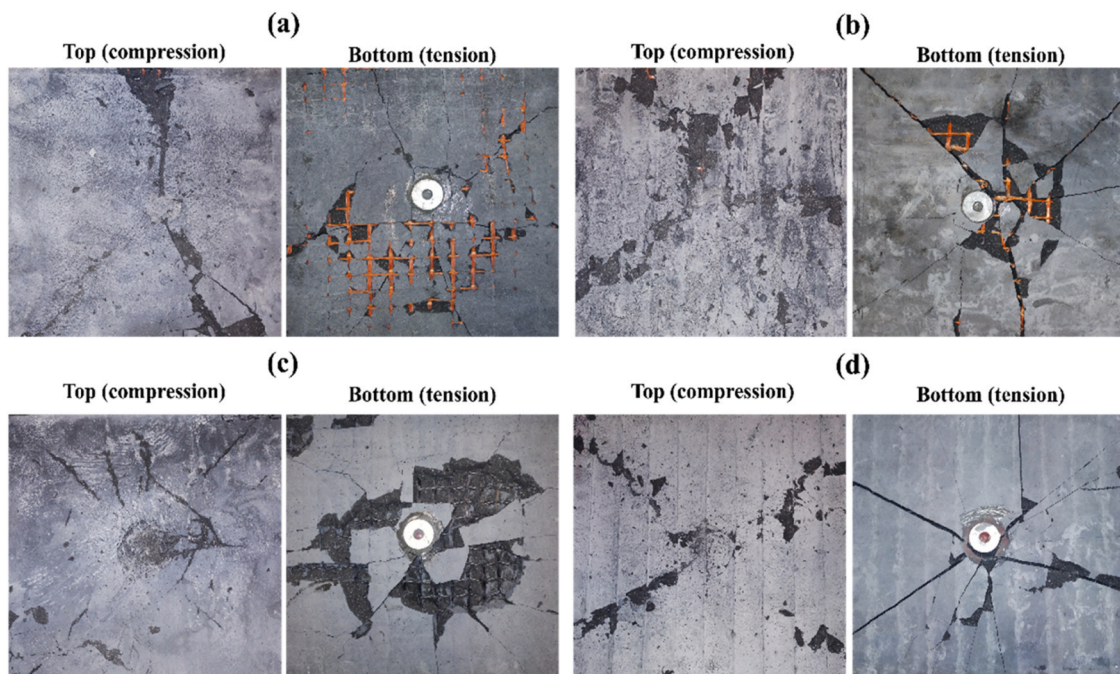


Fig. 16. : Top and bottom view of failure pattern after final impact (a) C-GT-H2 (b) P-GT-H2 (c) C-CT-H2 (d) P-CT-H2.

- However, under higher impact velocities, both AR-glass and carbon textile-reinforced specimens showed widened cracks and reduced impact resistance after 3 drops. The damage from higher velocity impacts is distributed better in the case of carbon textile-reinforced panels due to their enhanced composite behaviour and thus improves the energy absorption capacity and impact resistance when compared to AR-glass textile-reinforced specimens.
- In addition, the failure pattern shows that the AR-glass textile-reinforced panels had severe punching failure and widened cracks on the compressive side and four main cracks developed towards the support on the tension side along with significant spalling. However, providing high-strength carbon textile reinforcement improves the interlayer bridging for printed specimens and reduces the crack widening and spalling. Furthermore, the enhanced hardening behaviour improves the impact resistance capacity and forms multiple cracks on the tension side during failure.

Providing textile reinforcement was observed to show enhanced impact resistance and improve the energy absorption capacity of printed concrete panels significantly. This provides geometrical freedom to construct architecturally pleasing impact-resistant structures using textile-reinforced 3D concrete printing. However, further detailed investigation on the impact behaviour of 3D concrete printed specimens based on the effect of mesh size and area of textile reinforcement, optimised print path and higher impact velocities need to be studied.

#### CRedit authorship contribution statement

**Akilesh Ramesh:** Writing – original draft, Methodology, Investigation, Formal analysis, Data curation. **Guoxing Lu:** Resources, Data curation. **Jay Sanjayan:** Writing – review & editing, Supervision, Resources, Project administration, Methodology, Investigation, Conceptualization. **Shanqing Xu:** Writing – review & editing, Supervision, Resources, Investigation, Data curation. **Pathmanathan Rajeev:** Writing – review & editing, Supervision, Resources, Methodology, Investigation, Funding acquisition, Conceptualization.

#### Declaration of Competing Interest

The authors declare that they have no known competing financial interests or personal relationships that could have appeared to influence the work reported in this paper.

#### Data Availability

Data will be made available on request.

#### Acknowledgements

The authors gratefully acknowledge the financial support from the Australian Research Council Grant DP210101680 and LE170100168 for the research work reported in this paper. Further, the authors acknowledge KAST GmbH company, Germany, for providing textiles. The authors are greatly thankful to the staff of the Digital Construction Laboratory at the Swinburne University of Technology.

#### References

- [1] Gao W, et al. The status, challenges, and future of additive manufacturing in engineering. *Comput-Aided Des* 2015;69:65–89.
- [2] Buswell RA, et al. 3D printing using concrete extrusion: a roadmap for research. *Cem Concr Res* 2018;112:37–49.
- [3] Bos F, et al. Additive manufacturing of concrete in construction: potentials and challenges of 3D concrete printing. *Virtual Phys Prototyp* 2016;11(3):209–25.
- [4] Asprone D, et al. Rethinking reinforcement for digital fabrication with concrete. *Cem Concr Res* 2018;112:111–21.
- [5] Wangler T, et al. Digital concrete: a review. *Cem Concr Res* 2019;123:105780.
- [6] Mechtcherine V, et al. Integrating reinforcement in digital fabrication with concrete: a review and classification framework. *Cem Concr Compos* 2021;119:103964.
- [7] Perrot A, Rangedard D, Pierre A. Structural built-up of cement-based materials used for 3D-printing extrusion techniques. *Mater Struct* 2016;49:1213–20.
- [8] Sanjayan J, Jayathilakage R, Rajeev P. Vibration induced active rheology control for 3D concrete printing. *Cem Concr Res* 2021;140:106293.
- [9] Arunothayan AR, et al. Rheological characterization of ultra-high performance concrete for 3D printing. *Cem Concr Compos* 2023;136:104854.
- [10] Arunothayan AR, et al. Development of 3D-printable ultra-high performance fiber-reinforced concrete for digital construction. *Constr Build Mater* 2020;257:119546.
- [11] Murcia DH, Genedy M, Taha MR. Examining the significance of infill printing pattern on the anisotropy of 3D printed concrete. *Constr Build Mater* 2020;262:120559.
- [12] Ding T, et al. Anisotropic behavior in bending of 3D printed concrete reinforced with fibers. *Compos Struct* 2020;254:112808.
- [13] Arunothayan AR, et al. Fiber orientation effects on ultra-high performance concrete formed by 3D printing. *Cem Concr Res* 2021;143:106384.
- [14] Rajeev P, et al. Using Fibre recovered from face mask waste to improve printability in 3D concrete printing. *Cem Concr Compos* 2023;139:105047.
- [15] Marchment T, Sanjayan J. Mesh reinforcing method for 3D Concrete Printing. *Autom Constr* 2020;109:102992.
- [16] C. Scott, Chinese construction company 3D prints an entire two-story house on-site in 45 days. *3dprint.com*, 2016.
- [17] Hambach M, Rutzen M, Volkmer D. Properties of 3D-printed fiber-reinforced Portland cement paste. in *3D concrete printing technology*. Elsevier,; 2019. p. 73–113.
- [18] Pham L, Tran P, Sanjayan J. Steel fibres reinforced 3D printed concrete: Influence of fibre sizes on mechanical performance. *Constr Build Mater* 2020;250:118785.
- [19] Arunothayan AR, et al. Digital fabrication of eco-friendly ultra-high performance fiber-reinforced concrete. *Cem Concr Compos* 2022;125:104281.
- [20] Panda B, Paul SC, Tan MJ. Anisotropic mechanical performance of 3D printed fiber reinforced sustainable construction material. *Mater Lett* 2017;209:146–9.
- [21] Yang Y, et al. Mechanical anisotropy of ultra-high performance fibre-reinforced concrete for 3D printing. *Cem Concr Compos* 2022;125:104310.
- [22] Wu Z, Memari AM, Duarte JP. State of the art review of reinforcement strategies and technologies for 3D printing of concrete. *Energies* 2022;15(1):360.
- [23] Kim S, Kang TH, Hong S-G. Impact Performance of Thin Prefabricated Ultra-High-Performance Concrete Facade. *Acids Struct J* 2021;118(1):167–77.
- [24] Yoo D-Y, Bantbia N. Impact resistance of fiber-reinforced concrete-A review. *Cem Concr Compos* 2019;104:103389.
- [25] Hrynyk TD, Vecchio FJ. Behavior of steel fiber-reinforced concrete slabs under impact load. *Struct J* 2014;111(5):1213–24.
- [26] Ong K, Paramasivam P, Basheerkhan M. Behavior of Fiber-reinforced concrete slabs under low velocity projectile impact. *Spec Publ* 1999;172:993–1011.
- [27] Zhang J, Maalej M, Quek ST. Performance of hybrid-fiber ECC blast/shelter panels subjected to drop weight impact. *J Mater Civ Eng* 2007;19(10):855–63.
- [28] Valeri P, et al. Textile reinforced concrete for sustainable structures: Future perspectives and application to a prototype pavilion. *Struct Concr* 2020;21(6):2251–67.
- [29] Ehlig D, et al. Textile concrete - an overview of executed projects. *Beton-und Stahlbetonbau*, 107. Wiley Online Library,; 2012. p. 777–85.
- [30] Scholzen A, Chudoba R, Hegger J. Thin-walled shell structures made of textile-reinforced concrete: part I: structural design and construction. *Struct Concr* 2015;16(1):106–14.
- [31] Peled A, Bentur A, Mobasher B. Textile reinforced concrete, Vol. 19. CRC Press,; 2017.
- [32] de Andrade Silva F, et al. Strain rate effect on the tensile behaviour of textile-reinforced concrete under static and dynamic loading. *Mater Sci Eng: A* 2011;528(3):1727–34.
- [33] Zhu D, Gencoglu M, Mobasher B. Low velocity flexural impact behavior of AR glass fabric reinforced cement composites. *Cem Concr Compos* 2009;31(6):379–87.
- [34] Gopinath S, et al. Investigations on the influence of matrix and textile on the response of textile reinforced concrete slabs under impact loading. *Sādhanā* 2018;43:1–11.
- [35] Gopinath S, Prakash A, Ahmed AF. Flexural impact response and energy absorption characteristics of textile reinforced mortar. *Constr Build Mater* 2020;262:120630.
- [36] Li A, et al. Dynamic flexural behavior of AR-glass textile reinforced concrete under low-velocity impact loading. *J Sustain Cem-Based Mater* 2023;12(1):49–67.
- [37] Liu S, et al. Impact response of basalt textile reinforced concrete subjected to different velocities and temperatures. *Constr Build Mater* 2018;175:381–91.
- [38] Li A, et al. Dynamic flexural behaviors of AR-glass textile-reinforced concrete after exposure to elevated temperatures. *J Mater Civ Eng* 2023;35(12):04023453.
- [39] Liu S, et al. Flexural response of basalt textile reinforced concrete with pre-tension and short fibers under low-velocity impact loads. *Constr Build Mater* 2018;169:859–76.
- [40] Gopinath S, Prakash A, Ahmed AF. Synergy of hybrid textile reinforced concrete under impact loading. *Sādhanā* 2020;45(1):11.
- [41] van Rensburg JJ, Babafemi AJ, Combrinck R. A textile reinforcement method for 3D printed concrete. *MATEC Web Conf* 2022 (EDP Sciences).
- [42] Wang, W., et al. Flexural behaviour of AR-glass textile reinforced 3D printed concrete beams. in *Second RILEM International Conference on Concrete and Digital Fabrication: Digital Concrete 2020 2*. 2020. Springer.
- [43] Nikravan A, et al. Implementation of continuous textile fibers in 3D printable cementitious composite. *International Symposium of the International Federation for Structural Concrete*. Springer,; 2023.

- [44] Ramesh A, et al. In-process textile reinforcement method for 3D concrete printing and its structural performance. *Eng Struct* 2024;314:118337.
- [45] Liu C, et al. Anisotropic mechanical properties of extrusion-based 3D printed layered concrete. *J Mater Sci* 2021;56(30):16851–64.
- [46] Mo Y, et al. Dynamic Properties and Fractal Characteristics of 3D Printed Cement Mortar in SHPB Test. *Materials* 2021;14(19):5554.
- [47] Yang Y, et al. Characteristics of 3D-printing ultra-high performance fibre-reinforced concrete under impact loading. *Int J Impact Eng* 2022;164:104205.
- [48] Australia, S, AS 3972 general purpose and blended cements. Sydney, Australia: Standards Australia, 2010.
- [49] Australia, S, AS 3582.3 Supplementary cementitious materials for use with portland and blended cement. Sydney, Australia: Standards Australia, 2016.
- [50] Standard, A, C136, Standard Test Method for Sieve Analysis of Fine and Coarse Aggregates, ASTM International, West Conshohocken, PA, 2006.
- [51] Australia, S, AS 1478.1 Chemical admixtures for concrete, mortar and grout-admixtures for concrete. Sydney, Australia: Standards Australia, 2000.
- [52] ASTM-C1437, Standard test method for flow of hydraulic cement mortar. ASTM, 2007.
- [53] Feys D, et al. Extension of the Reiner–Riwlin equation to determine modified Bingham parameters measured in coaxial cylinders rheometers. *Mater Struct* 2013; 46:289–311.
- [54] Muthukrishnan S, Ramakrishnan S, Sanjayan J. In-line activation of geopolymer slurry for concrete 3D printing. *Cem Concr Res* 2022;162:107008.
- [55] Bong SH, et al. Method of formulating 3D-printable strain-hardening alkali-activated composites for additive construction. *Cem Concr Compos* 2022;134: 104780.
- [56] Ramesh A, Rajeev P, Sanjayan J. Bond-slip behaviour of textile-reinforcement in 3D printed concrete. *J Build Eng* 2024:108873.
- [57] Ranade R, et al. Impact resistance of high strength-high ductility concrete. *Cem Concr Res* 2017;98:24–35.
- [58] Reid JD, et al. Inertial effects during impact testing. *Transp Res Rec* 2009;2120(1): 39–46.